J Fail. Anal. and Preven. (2015) 15:750–757
DOI 10.1007/s11668-015-0013-x

TECHNICAL ARTICLE—PEER-REVIEWED

Failure Analysis of a Low-Pressure Turbine Blade in a Coal-Based Thermal Power Plant

M. Ananda Rao · M. V. Pavan Kumar · T. S. N. Sankara Narayanan · S. Subba Rao · N. Narasaiah

Submitted: 8 April 2015 / in revised form: 18 August 2015 / Published online: 8 September 2015

Abstract The failure of a turbine blade of a 60 MW thermal power plant is addressed in this paper. The findings of this study, based on the operating conditions and the characteristics of failed turbine blade, suggest a corrosion fatigue-related failure. The paper addresses the key elements that could have possibly lead to the failure of the turbine blade and highlights the importance of scrutinizing the operating conditions to eliminate the occurrence of such failures.

Keywords Turbine blade failure · Thermal power plant · Corrosion fatigue · Fractography

M. Ananda Rao (✉) · S. Subba Rao
CSIR-National Metallurgical Laboratory, Madras Centre, CSIR Complex, Taramani, Chennai 600 113, India
e-mail: anandm04@gmail.com

S. Subba Rao
e-mail: sripadas@gmail.com

M. V. Pavan Kumar
Department of Chemical Engineering, National Institute of Technology Calicut, Kozhikode, India
e-mail: malladi@nitc.ac.in

T. S. N. Sankara Narayanan
Department of Dental Biomaterials and Institute of Biodegradable Materials, Chonbuk National University, Jeonju 561-756, South Korea
e-mail: tsnsn@rediffmail.com

N. Narasaiah
Department of Metallurgical and Materials Engineering, National Institute of Technology Warangal, Warangal, India
e-mail: narasaiahn@yahoo.co.in

Introduction

The efficiency and longevity of a thermal power plant predominantly depends on the prevention of the steam turbine blade failures [1–3]. Material defects, high/low cycle fatigue, corrosion induced by associated extreme operating conditions, high stresses, the presence of crevices that are conducive to the condensation of the concentrated solutions of steam contaminants, and improper feed water chemistry are regarded as the root causes for the failures of steam turbine blades [4, 5]. Several case studies on steam turbine blade failures were reported earlier [6–13]. The failures of low-pressure (LP) steam turbine blades are more common (~40%) in comparison to that of high or intermediate pressure turbines [6].

In the present work, the failure of a LP steam turbine blade is investigated. The blade was present in 3A stage of a LP steam turbine of a 60 MW thermal power plant located in India. The failure of the blade occurred prematurely after 9350 h of service. The main objective here is to identify the root cause of the failure and analyze the same while emphasizing the water/steam chemistry, as well as working conditions prior to the failure.

Experimental Procedure

X-ray radiography with 225 k V radiographic tester (Siefert, Germany) that has a resolution of 1.5% of the thickness of the sample is used to find any internal cracks or voids, inside the ripped off blade. The chemical composition of the failed blade sample was analyzed using optical emission spectrometer (OES) (Model: Spectrolab, Germany). Surface characteristics of the failed blade were

analyzed using stereo microscopy (Model: Leica, Switzerland). A blade sample that consists of the actual failed plane in its one end was made ready for further tests. The nature and composition of the deposits on the blade and impurities in the boiler water at different locations were tested using conventional wet chemical methods and atomic absorption spectrometer (AAS, Model: GBC Avanta), respectively. The microstructure of the sample was assessed using optical microscopy (Model: Leica, DMLM Switzerland) after etching. Fractographic analysis was performed using scanning electron microscopy (SEM) (Model: JEOL JSM 739A) to ascertain the nature of failure. Energy dispersive spectroscopy analysis (EDS) was performed to determine the chemical nature of the surface deposits. Hardness measurements were carried out using Brinell Hardness testing machine (B3000H) as Brinell hardness number (BHN) with 3000 kg load.

Results and Discussion

Visual Examination

The failure happened as the blade breaking into two pieces with one piece attached to the rotor. A schematic of the failed turbine blade with the plane of fracture is shown in Fig. 1. As the first step of the analysis, the failed blade is visually examined. A photograph of the ripped off turbine blade piece in its as-received condition is shown in Fig. 2(a). The color of the surface of the blade was black. Of this figure, the highlighted (encircled) portion is shown in Fig. 2(b), i.e., the sample carved out of the failed blade for further analysis. From Fig. 2(b), it can be observed from the slightly perceivable beach marks on the fractured surface that the crack was initiated at the leading edge of the aerofoil region encircled in the figure. The other fractured surface (on the right side of encircled portion area) appears to be gradually detached portion due to fatigue prior to the ultimate failure with plastic deformation at the trailing edge. The corrosion deposits present on the fractured surface are shown in Fig. 2(c), and the region where the stereo micrograph is captured is indicated with an arrow in Fig. 2(b).

Chemical Analysis, X-ray Radiography, and Hardness

The chemical composition of the blade, analyzed using an OES, is given in Table 1. The composition of the blade matches with that of the manufacturer's standard material composition for X22CrMoV12-1 alloy as per BS EN 10269 [14]. The X-ray radiographic images of the failed blade sample shown in Fig. 3 clearly reveal that there are no internal defects such as pores, voids, microcracks, etc., in the blade. Hence, the possibility of failure, due to material defects and internal defects like pores, voids, microcracks, etc., is ruled out. It can be noted that radiography technique can detect an internal defect of size up to 10 μm [15, 16]. The measured hardness of the failed blade is found to be in

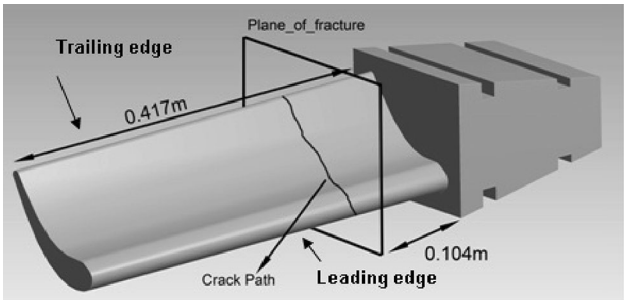

Fig. 1 Schematic diagram of the failed turbine blade indicating its fracture path

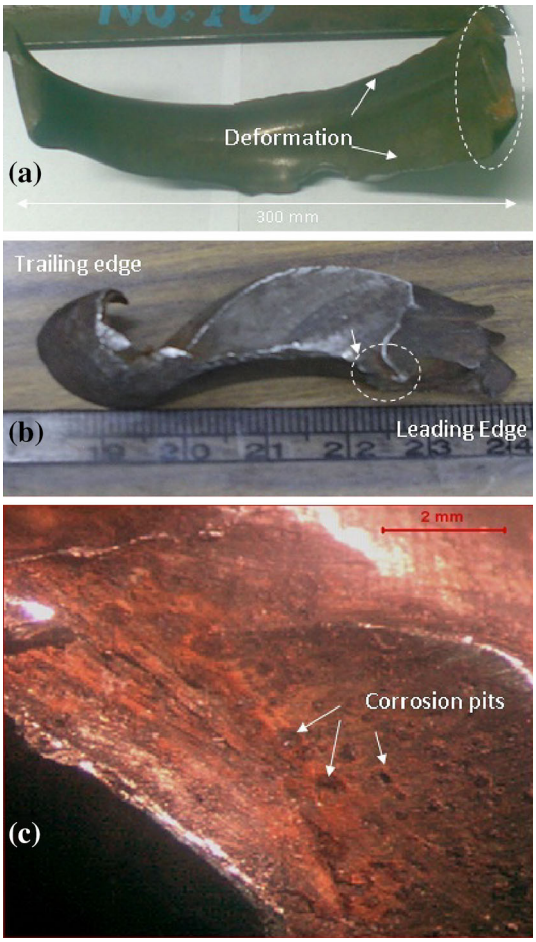

Fig. 2 Photographs of failed blade (**a**) in as-received condition (**b**) piece of blade used for analysis (highlighted in (**a**)), and (**c**) stereo micrograph taken along the along the fractured region edge (highlighted in (**b**))

Table 1 Chemical composition of the failed turbine blade

Element (wt.%)	C	Mn	P	S	Si	Ni	Cr	Mo	V	Fe
Failed blade	0.21	0.61	0.013	0.003	0.21	0.61	11.10	1.00	0.25	Bal.
X22CrMoV12-1	0.18–0.24	0.30–0.80	0.035	0.035	0.10–0.50	0.30–0.80	11–12.5	0.8–1.2	0.25–0.30	Bal.

Fig. 3 (**a**) X-ray radiography images of the failed blade, 80 kV × 5 mA (**b**) photograph of as-received failed blade

the range of 238–242 BHN and matches with the manufacturer's standard turbine blade material (X22CrMoV12-1) hardness (240–290 BHN) [17].

Microscopy

A Stereo micrograph taken along the leading edge of the aerofoil section on the convex curvature of the blade is shown in Fig. 4(a). Severe erosion marks can be seen in this figure. Also, the stereo micrograph taken on the surface of the convex curvature of the blade nearby trailing edge exhibited severe erosion features as shown in Fig. 4(b). Erosion is generally characterized by grooves and patterned wave-like formations on the surface, while pit corrosion is characterized as small holes on the surface with corrosion deposits. No corrosion features were observed on the convex curvature regions of the blade toward the leading edge; however, the regions were severely affected by erosion. In case of LP steam turbines, it was reported that the leading edge of the blade is more prone to erosion by water drops in the wet steam [4]. Erosion is also possible by the impingement of silica carried by the steam [7]. The stereo micrograph images taken on the concave curvature of the blade at leading and trailing edges are shown in Fig. 4(c), (d) respectively. Several corrosion pits can be seen in these images. The micrograph shown in Fig. 4(c) depicts the features of both erosion and corrosion. From this analysis, it can be said that the concave side surface of the blade at the leading edge suffered from both erosion and corrosion. Erosion causes the grooves to form, and corrosive agents deposit inside the grooves to further weaken the blade at the leading edge, particularly on the concave curvature side surface. Note that in Fig. 2(b), the highlighted failure initiation point is on the concave curvature side surface.

The alloy X22CrMoV12-1 is a variety of high-temperature-resistant steels with 12% Chromium and is employed as manufacturing material for steam turbine blades [18]. At higher temperatures, these materials are highly prone to erosion by flaked-off particles [19] and corrosion-induced fatigue [20]. The microstructure of the blade consisted of tempered martensite, as shown in Fig. 5. This meets the manufacturer's specifications of the material on such applications [21]. However, traces of carbides are seen at higher magnifications (Fig. 6). No degradation in the microstructure of the blade was observed.

Fractography

A few scanning electron micrographs of the failed turbine blade taken at the fatigue crack initiation point (see Fig. 2b) are shown in Fig. 7. EDS analysis performed at this region indicates the presence of silicon and chlorine as predominant foreign elements. The scanning electron micrographs arranged in such a way to see along the direction of crack growth, and to reveal the presence of beach marks on the fractured surface which is a typical characteristic feature of a failure due to fatigue [22]. Hence, that the turbine blade undergoing repeated cyclic loadings before the ultimate failure becomes conclusive. Sometimes, the crack initiation point due to corrosion fatigue can be in the aerofoil region of the trailing edge also [7]. However, the location where the corrosive agents accumulate inside the grooves subsequent to the erosion of

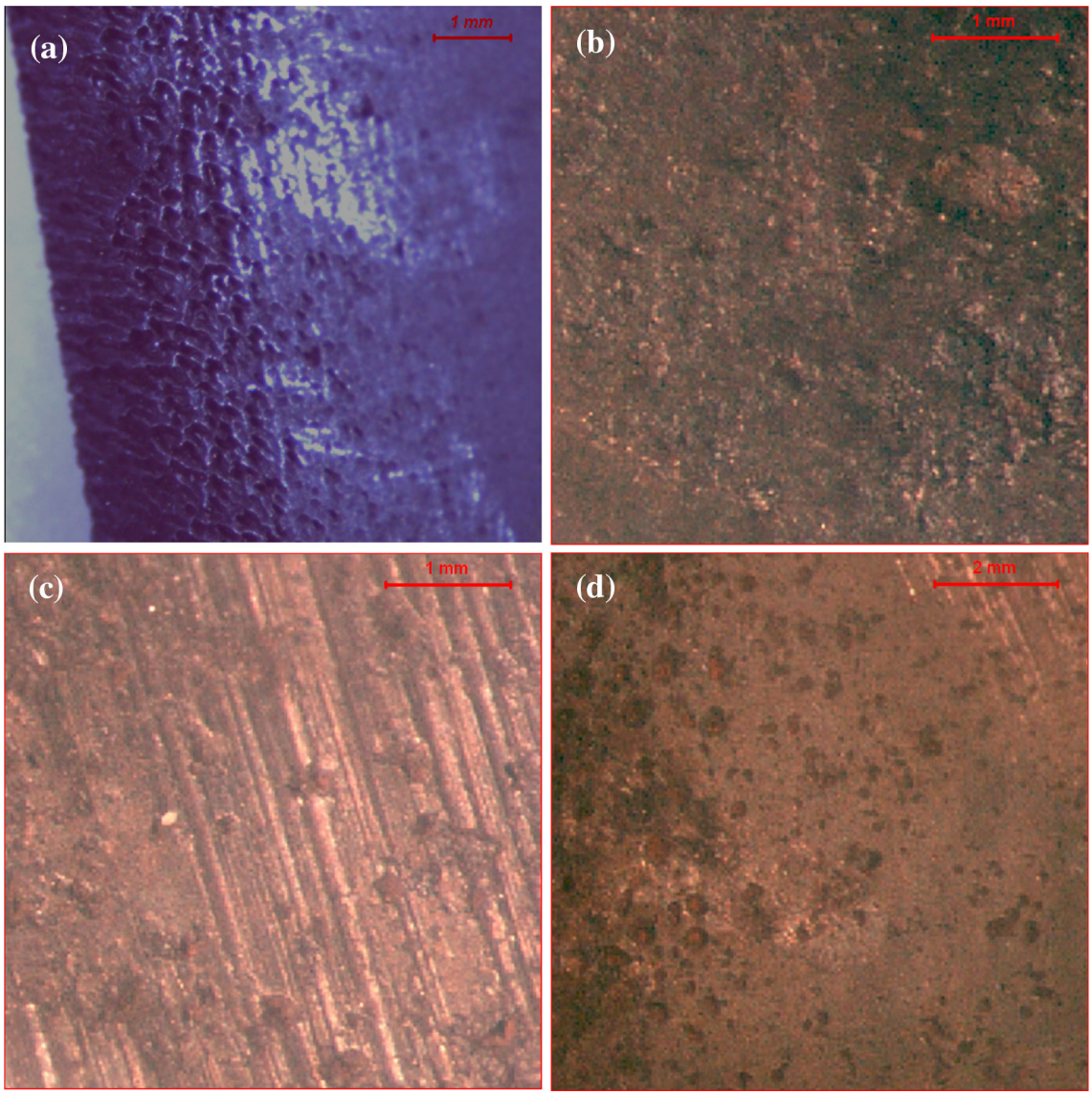

Fig. 4 Stereo micrograph taken on the surface of the blade at (**a**) along the leading edge, convex side (**b**) near trailing edge, convex side, (**c**) on the leading edge concave side and (**d**) near trailing edge, concave side

the surface is very much critical for inducing corrosion-induced fatigue.

A scanning electron micrograph of the irregular pits on the edge of fractured surface is given Fig. 8. Bulk EDS analysis performed at a pit region reveals surface oxidation and the presence of chlorine, silicon, potassium, and calcium as extraneous elements besides iron as shown in Table 2. The results of the analysis conducted at a location away from the pit are also presented in Table 2. Pitting is commonly associated with chloride deposits along with sodium hydroxide, sulfate, and sulfides [23]. The source of deposits on the turbine blade is the impurities in the water in the form of salts and silica in the boiler water. As steam enters and expands through the turbine, the solubility of contaminants in the steam decreases and they condense on the surfaces at solution concentrations higher than that of the original contaminant concentration in the steam [4, 24]. Once these contaminants accumulate in the grooves formed by erosion of the surface by silica and water droplets present in the steam, they promote pitting corrosion of the turbine blade.

Samples of the corrosion products and deposits on the fracture surface were collected for analysis. Conventional wet chemical analysis of the deposit sample confirms the presence of notable amounts of chlorides (29.08%) and silica (11.18%) (Table 3). The presence of iron oxides (38.01%) in the deposit is due to the oxidation of turbine blade. The only source of these deposits is the impurities present in the boiler feed water. Thus, the boiler feed water

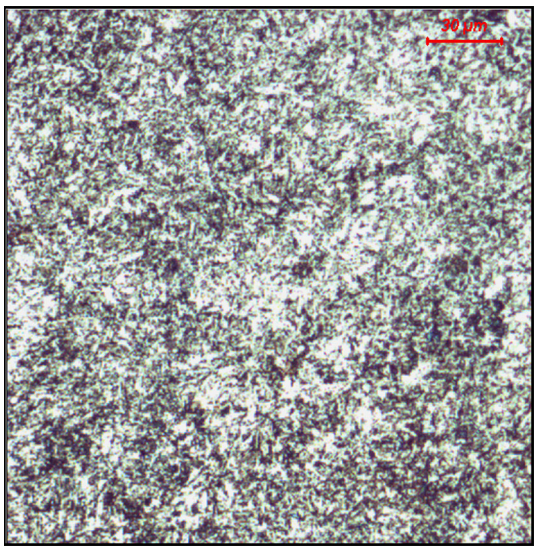

Fig. 5 Optical microstructure of the blade at the failed region (tempered martensite)

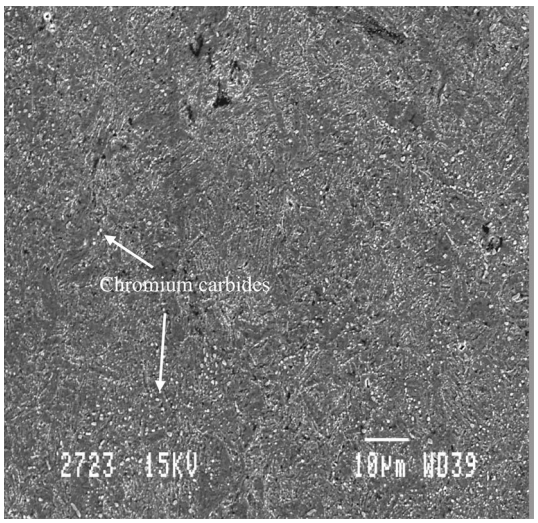

Fig. 6 SEM image of the martensite matrix highlighting the presence of carbide precipitation (white color) with white arrows

samples at different location are collected to find the impurities present.

A schematic of the boiler with water flow directions is shown in Fig. 9. The AAS analysis of the water samples collected from three different locations of the boiler namely, boiler blow down, boiler drum steam, and feed water shows the presence of significant amounts of M-alkalinity, chlorine, and silicon (Table 4). It is well known that the presence of chlorine facilitates the localized corrosion attack in the form of pits. Considering the characteristic feature of the failure such as beach marks and pits observed in SEM analysis coupled with the

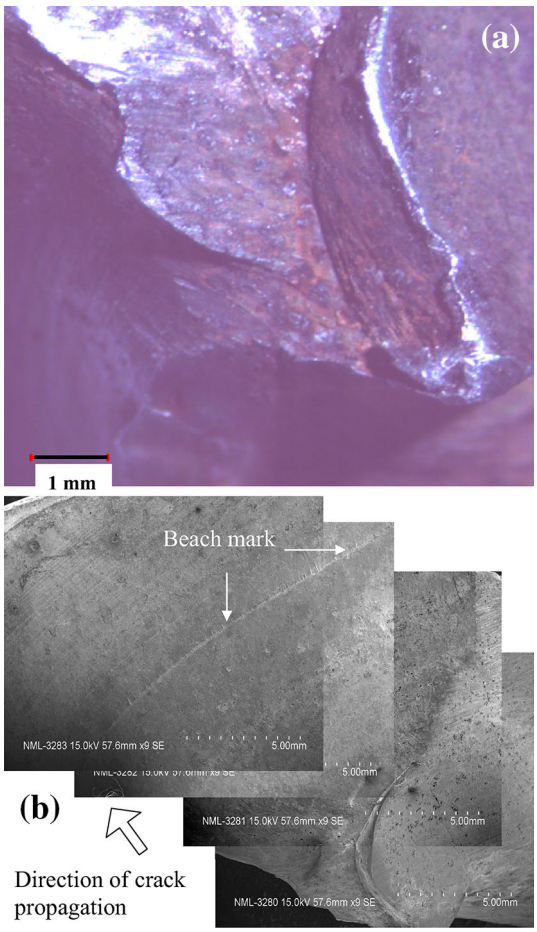

Fig. 7 (**a**) Stereo micrograph of crack initiation point and (**b**) Sequence of scanning electron micrographs show the crack propagation

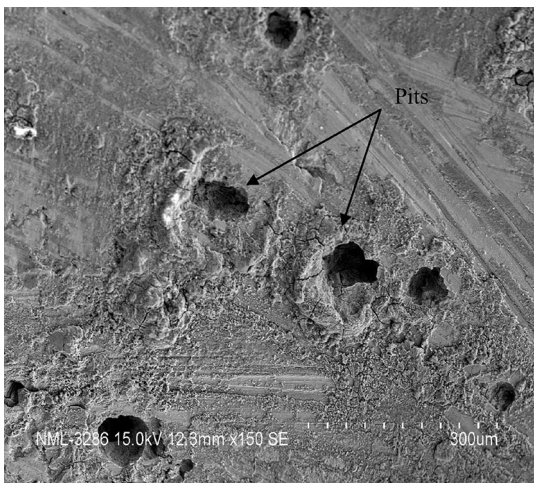

Fig. 8 Scanning electron micrograph taken on the fractured surface at the crack initiation point showing corrosion pits

accumulation of the deposits containing significant amounts of chloride and silica, it is quite obvious that the mode of failure of the turbine blade is due to corrosion-induced fatigue, which is also referred as corrosion fatigue. The formation of grooves of appreciable size by the erosion and the presence of corrosive agents such as chlorine followed by severe localized stress concentrations have led to the failure. In the current work, the nature of corrosion is pitting type due to the accumulation of chlorine in the pits formed due to the erosion.

Table 2 Bulk EDS chemical analysis at a pit and away from the pit (Fig. 8)

Element	On the pit wt.%	Away from the pit wt.%
O	14.46	11.86
Na	0.38	0.30
Al	1.01	···
Si	1.95	0.71
S	···	0.40
Cl	2.05	0.38
K	0.98	0.56
Ca	1.12	0.83
Cr	3.55	12.79
Fe	74.50	71.19
Ni	···	0.97

Table 3 Composition of the deposits analyzed by wet chemical analysis technique

Element	Concentration (wt.%)
Moisture	0.74
Loss on ignition	1.58
Iron as Fe_2O_3	38.01
Aluminum as Al_2O_3	0.36
Magnesium as MgO	1.40
Calcium as CaO	6.13
Potassium as K_2O	0.006
Copper as CuO	0.0056
Phosphorous as P_2O_5	0.33
Sodium as Na_2O	11.08
Chlorine as Chlorides	29.08
Silica as SiO_2	11.18

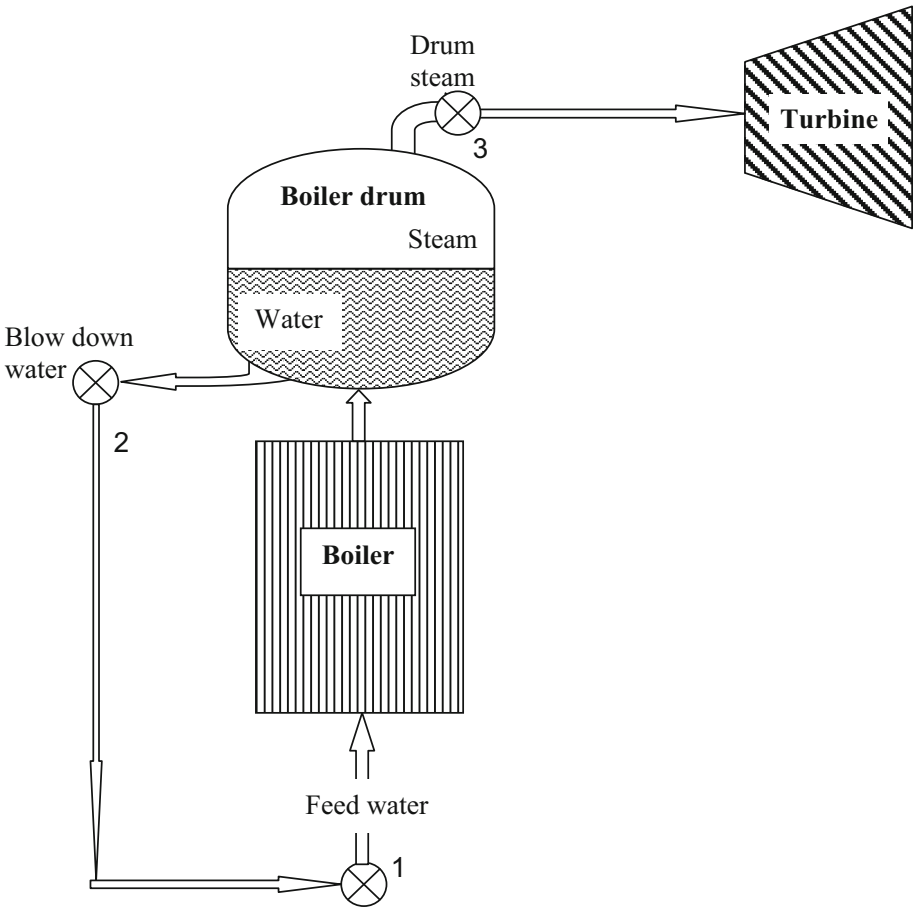

Fig. 9 Schematic diagram of the boiler and turbine assembly showing the feed water, boiler blow down water, and boiler drum steam locations

Table 4 Chemical analyses of the water samples using the wet chemical analysis technique

	Boiler drum steam	Boiler blow down water	Feed water (DM water)
pH	8.9	9.2	7.0
Chloride	12 ppm	35 ppm	5 ppm
Silica	20 ppb	0.2–0.8 ppm	8–12 ppb
M-Alkalinity	3 ppm	8–10 ppm	20–30 ppm

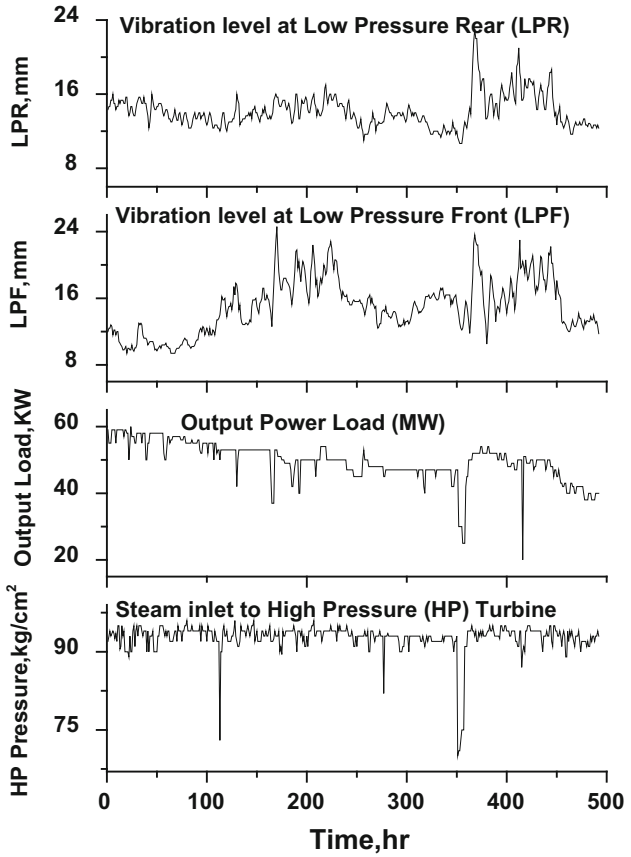

Fig. 10 Variation in turbine inlet steam pressure (HP inlet), output power load, and vibration levels recorded at the front (LPF) and rear (LPR) of the turbine as a function of time

Analysis of Operational Conditions of the Turbine

Some salient working conditions during the operation of the turbine system (includes both HP (high pressure) and LP turbines) were also examined to see if any relation exists between these and mode of failure. Prior to the failure, for 492 h, the vibration levels at the front and rear of the LP region of the steam turbine, the output power load, and the inlet steam pressure to the HP turbine were examined. A sudden substantial drop in the inlet pressure from ~95 to ~73 kg/cm^2, followed by sudden reversal to ~95 kg/cm^2 at around 113–117 h is observed. In addition, several fluctuations (~351 to 357, ~415 h) of varying levels in the inlet pressure could be noticed. The safety limit of inlet pressure of the steam entering into the turbine was defined as ~92 kg/cm^2. However, the average inlet pressure condition is well over ~92 kg/cm^2 suggesting that the safe operational limit was deviated during the operation of the turbine. The fluctuations in the output power load and HP inlet pressure measured as a function of time suggest the existence of a reasonable relation between them. Overall, the analysis implies that the failed turbine blade underwent uneven loading conditions due to variation in inlet pressure.

The vibration levels are also indicators of the deviations in the operational conditions. The vibration levels recorded at low-pressure front (LPF) and low-pressure rear (LPR) regions of the LP turbine as a function of time for 492 h are shown in Fig. 10. Also given are the HP inlet steam pressure and output load of the turbine. For the disturbance in HP inlet steam pressure at 113–117 h, vibrations in LPF can be observed with no such vibrations at LPR. However, as the time progressed, both LPF and LPR showed similar vibrations. This could be due to the onset of the failure of the blade. Note that the average levels of vibrations in LPF and LPR are increased with the time. The onset of failure can amplify the vibrations and the blades further undergo heavy loading. However, such phenomena are not seen in the case but the change in the vibration is observed in response to changes in HP inlet pressure only. It is an evidence of the occurrence of frequent overloading due to the changes in HP inlet steam. The sudden loading and unloading phenomenon on the blade, together with the constant operation of the turbine in overloaded condition and vibration fluctuations, is considered to be critical in culminating the failure.

Conclusions

The chemical, hardness, and radiographic analyses confirm that the possibility of failure of the turbine blade due to improper material selection and internal material defects is ruled out. The tempered martensite structure of the failed blade confirms that it was operated within its safe limits of temperature. The erosion of the surface by silica followed by the deposition of corrosive ions in the grooves thus formed on the concave curvature side aerofoil section at the leading edge has thus weakened the blade strength. The presence of corrosive species like chlorine in the form of chlorides facilitates localized corrosion attack in the form of pits, leading to formation of cracks of appreciable size

under severe localized stress concentrations. Due to the fluctuations in working conditions, the corrosion fatigue ultimately led to the failure. The characteristic features of the failure such as beach marks and pits coupled with the accumulation of deposits containing significant amounts of chloride and silica confirm that the mode of failure of the turbine blade is due to corrosion-induced fatigue, which is also referred as corrosion fatigue.

Acknowledgments The authors express their sincere thanks to Director, CSIR-National Metallurgical Laboratory, Jamshedpur, for his valuable guidance, encouragement, and permission to publish this work.

References

1. H.G. Naumann, Steam turbine blade design options: how to specify or upgrade, in *Proceedings of the Eleventh Turbomachinery Symposium*, (A& M University Press, College Station, Texas, TX 1982), pp .29–50
2. R. Viswanathan, *Damage mechanisms and life assessment of high temperature components* (Metals Park, ASM International, 1989), p. 313
3. A. Atrens, H. Meyer, G. Faber, K. Schneider, M.O. Speidel, A. Atrens, *Corrosion in Power Generating Equipment* (Plenum Press, Metals Park, 1983), p. 299
4. O. Jonas, L. Machmer, Steam turbine corrosion and deposits problems and solutions, in *Proceedings of Thirty Seventh Turbomachinery and Symposium*, 2008, pp. 211–227
5. J.S. Sohre, Steam turbine blade failures, causes and correction, in *Proceedings of the 4th Symposium Turbomachinery Symposium*, (A& M university, Texas, 1975), pp. 9–30
6. N.K. Mukhopadhay, S. Ghosh Chowdhury, G. Das, I. Chottoraj, S.K. Das, D.K. Battacharya, An investigation of the failure of low pressure steam turbine blades. Eng. Fail. Anal. **5**, 181–193 (1998)
7. G. Das, S. Ghosh Chowdhury, A.K. Ray, S.K. Das, D.K. Battacharya, Turbine blade failure in a thermal power plant. Eng. Fail. Anal. **10**, 85–91 (2003)
8. D. Ziegler, M. Puccinelli, B. Bergallo, A. Picasso, Investigation of turbine blade failure in a thermal power plant, Case Studies. Eng. Fail. Anal. **1**, 192–199 (2013)
9. B.M. Schonbauer, A. Perlega, and S.E. Stanzl-Tschegg, Pit to crack transition and corrosion fatigue of 12% Cr steam turbine blade steel, in *13th International Conference on Fracture*, 2013, pp. 16–21
10. Nurbanasari and Abdurrachim, Crack of a first stage blade in a steam turbine case studies. Eng. Fail. Anal. **2**, 54–60 (2014)
11. A. Turnbull, Current understanding of environment-induced cracking of steam turbine steels. Corrosion **64**(5), 420–438 (2008)
12. C.R.F. Azevedo, A. Sinatora, Erosion-fatigue of steam turbine blades. Eng. Fail. Anal. **16**(7), 2290–2303 (2009)
13. J. Kubiak, G. Gongalez, D. Juarez, J. Nebradt, F. Sierra et al., J. Fail. Anal. Prev. **4**(3), 47–51 (2004)
14. Chemical compositions of stainless steel BS EN 10269, Featured articles and publications, European EN grade summary, British stainless steel Association, Pegasus House, Sheffield
15. Development of protocols for corrosion and deposits evaluation in pipes by radiography, International Atomic Energy Agency-TECDOC-1445, Austria, 2005, pp. 9–10
16. W. Clay, Maranville "Radiographic imaging of microstructural defects in ceramic tapes", Retrospective Theses and Dissertation, Lowa State University, Ames, 1996
17. "Turbine inspection manual" M/s SKODAPOWER—OEM—Czech Republic, 2005
18. C. Leinenbach, A. Al-Badri, M. Roth, M. Hadad, S. Siegmann, B. Scarlin, M. Staubli, R. Hitzek, P. Bürgler, A. Nicoll, R. Damani, Th. Peters, J. Crummenauer, G. Reisel, Coatings for valves and blades in steam turbines, EPMA publications, 2007, EPMA-20070344
19. Bernd M. Schönbauer, Andrea Perlega, Stefanie E. Stanzl-Tschegg, Pit-to-crack transition and corrosion fatigue of 12% Cr steam turbine blade steel, in *13th International Conference on Fracture*, Beijing, China, 2013, pp. 1–10
20. K.M. Perkins, M.R. Bache, Corrosion fatigue of a 12%Cr low pressure turbine blade steel in simulated service environments. Int. J. Fatigue **27**, 1499–1508 (2005)
21. A.K. Bhaduri, T.P.S. Gill, S.K. Albert, K. Shanmugam, D.R. Iyer, Repair welding of cracked steam turbine blades using austenitic and martensitic stainless-steel consumables. Nucl. Eng. Des. **206**, 249–259 (2001)
22. G.E. Totten, Fatigue crack propagation. Adv. Mater. Proc. **166**(5), 39–41 (2008)
23. Yuichi Yoshino, Akihiko Ikegaya, Pitting and stress cracking of 12Cr–Ni–Mo martensitic stainless steels in chloride and sulfide environments. Corrosion **41**(2), 105–113 (1985)
24. Alireza Bahadori, Hari B. Vuthaluru, Prediction of silica carry-over and solubility in steam of boilers using simple correlation. Appl. Therm. Eng. **30**, 250–253 (2010)